A nonlinear model order reduction approach to the elastohydrodynamic problem

D. Maier [a,*], C. Hager [a], H. Hetzler [b], N. Fillot [c], P. Vergne [c], D. Dureisseix [c], W. Seemann [b]

[a] Department of Structural and Contact Dynamics, Corporate Sector Research and Advanced Engineering, Robert Bosch GmbH, 70049 Gerlingen-Schillerhöhe, Germany
[b] Institute of Engineering Mechanics (ITM), Karlsruhe Institute of Technology (KIT), 76131 Karlsruhe, Germany
[c] Université de Lyon, INSA-Lyon, LaMCoS, CNRS, UMR5259, F-69621 Villeurbanne Cedex, France

ARTICLE INFO

Keywords:
Elastohydrodynamic lubrication
Reduced order model
Transient
Line contact

ABSTRACT

A model order reduction procedure is derived for the elastohydrodynamic (EHD) problem, Reynolds and elasticity part, to increase the calculation speed. The method is derived for stationary and transient isothermal Newtonian line and point contacts. The reduction of the EHD contact model with exit boundary condition is performed in three steps. The first is a reduction of the system by projection using proper orthogonal decomposition. Within the second step, the complexity of system functions is reduced. The last reduces the computational costs for the exit boundary problem by employing a local scheme. Furthermore, a contact size related nondimensionalization is introduced. The method allows for considerable reduction of the calculation time while achieving excellent correspondence to results obtained by other approaches.

1. Introduction

The behavior of highly loaded lubricated contacts is of interest in many applications such as in cam tappet contacts or rolling element bearings. Nevertheless, there are cases within the process of designing where a classical full EHD calculation is too time consuming.

Thus, several works have dealt with getting relevant informa tion of typical EHD outputs without doing full calculations. Probably the most common approach has been the creation of design charts [1 3] in dependency of comparison parameters [4 6].

However, for the transient case, design charts are not easily applicable, since the solution depends on the past. Another procedure has been the derivation of simplified semi analytical models, which approximate the dynamic behavior of the full problem under specified conditions. Central film thickness fluc tuations have been studied in a dynamically loaded configuration, by using an Ertel Grubin scheme [7] and taking into account squeeze film effects [8] and effects due to a changing contact size [9].

* Corresponding author. Tel.: +49 711 811 38417.
E-mail address: daniel.maier6@de.bosch.com (D. Maier).

Another approach has been to approximate the nonlinear behavior of an EHD contact by an interpolation between the two limiting cases of a dry Hertzian contact and a purely hydrody namic contact [10].

Recently, first attempts have been taken to reduce the calcula tion time by applying model order reduction techniques to the structural part of the problem [11,12]. Nevertheless, since the highly non linear fluid part is not reduced within these approaches, the size and complexity of the problem to be solved is still large.

Within this work, not only the linear elasticity part of the problem will be reduced, but also the highly nonlinear part, representing the Reynolds equation [13]. Thus the necessary calculation time is strongly decreased, enabling the use of EHD contacts in a wider range of applications. Section 2 shows the underlying mathematical model, which gets reduced in Section 3. The results are given in Section 4, followed by a discussion and a conclusion.

2. Mathematical model

The isothermal Newtonian EHD contact on the domain Ω is given by the Reynolds equation with exit boundary condition, the elasticity equation and the load balance. Assuming only vertical displacements of the surfaces, the general form of the Reynolds

Nomenclature

Δ	dimensionless deformation
δ	elastic deformation
$\boldsymbol{\delta}_j$	deformation vector
η	viscosity
$\overline{\eta}$	dimensionless viscosity
Λ	dimensionless Lagrangian multiplier
λ	Lagrangian multiplier
$\boldsymbol{\lambda}_j$	Lagrangian multiplier vector
$\boldsymbol{\mu}_j$	parameter vector at jth time step
Ω	computational domain
ω	Newton damping coefficient
$\partial\Omega$	boundary of computational domain
ρ	density
$\overline{\rho}$	dimensionless density
a	Hertzian half width/radius
$\boldsymbol{D}$	pre conditioning diagonal matrix
E'	reduced modulus of elasticity
$\boldsymbol{f}_{\delta,j}$	discrete elasticity equation
$f_{h_{0j}}$	discrete load balance
$\boldsymbol{f}_{\boldsymbol{p}j}$	discrete Reynolds equation
$\boldsymbol{g}$	grid transformation function
H	dimensionless film thickness
h	film thickness
H_0	dimensionless rigid body displacement
h_0	rigid body displacement
K	flexibility matrix
m	number of snapshots
n	number of inner nodes
$\tilde{n}$	degrees of freedom of reduced system
$\hat{n}$	number of nonlinear function evaluations
$\check{n}$	number of necessary state vector entries
$\tilde{n}_\delta$	number of basis functions for deformation
$\tilde{n}_p$	number of basis functions for pressure
P	dimensionless pressure
p	pressure
$\boldsymbol{p}_j$	pressure vector
R	radius of curvature
T	dimensionless time
t	time
U	dimensionless mean velocity
u_m	mean surface velocity
$\boldsymbol{V}$	trial basis
$\boldsymbol{W}$	test basis
w	load
X, Y	dimensionless coordinates
x, y	coordinates
$\boldsymbol{z}_j$	state vector
$\mathcal{A}$	active set
$\mathcal{B}$	set of exit boundary nodes
$\mathcal{I}$	set of indices of nonlinear function evaluations
$\mathcal{J}$	set of evaluated state vector entries
$\mathcal{P}$	passive set
$\tilde{\mathcal{P}}$	passive set for Reynolds equation only

equation may be formulated as a complementarity problem (CP) according to

$$\left.\begin{cases} \frac{\partial}{\partial x}\left(\frac{\rho h^3}{12\eta}\frac{\partial p}{\partial x}\right)+\frac{\partial}{\partial y}\left(\frac{\rho h^3}{12\eta}\frac{\partial p}{\partial y}\right)+\lambda = u_m\frac{\partial \rho h}{\partial x}+\frac{\partial \rho h}{\partial t}, \\ \lambda \geq 0,\ p \geq 0,\ \lambda \cdot p = 0 \end{cases}\right\} \quad \text{in } \Omega$$

$$p = 0 \quad \text{on } \partial\Omega. \tag{1}$$

Here, $p(x,y,t)$ is the pressure, u_m the mean velocity of the two surfaces and λ the Lagrangian multiplier, which is introduced to enforce the unilateral constraint $p \geq 0$. The film thickness h is a superposition of the rigid body approach h_0, the gap $(x^2+y^2)/2R$ between the undeformed contours of the bodies and the deformation δ:

$$h(x,y,t) = h_0(t) + \frac{x^2+y^2}{2R} + \delta(x,y,t). \tag{2}$$

For a line contact problem, all terms including y are discarded in (1) and (2). The relation between fluid pressure and load is given by the load balance. It reads

$$\int_{-\infty}^{+\infty} p(x)\,dx = w \quad \text{or} \quad \int_{-\infty}^{+\infty}\int_{-\infty}^{+\infty} p(x,y)\,dx\,dy = w, \tag{3}$$

for a line or a point contact, respectively. Finally, considering the two elastic bodies as a half space, the elastic deformation can be given for a line contact by [14]

$$\delta(x,t) = \frac{2}{\pi E'}\int_{-\infty}^{+\infty} p(x',t)\ln\left(\left(\frac{x-x'}{a}\right)^2\right)dx' + C(t), \tag{4}$$

and for a point contact by [15]

$$\delta(x,y,t) = \frac{2}{\pi E'}\int_{-\infty}^{+\infty}\int_{-\infty}^{+\infty}\frac{p(x',y',t)\,dx'\,dy'}{\sqrt{(x-x')^2+(y-y')^2}}. \tag{5}$$

The integration constant C in Eq. (4) is added to h_0 in Eq. (2). Density ρ and viscosity η can be dependent on pressure.

2.1. Nondimensionalization

Next, the problem will be transformed into dimensionless form, in order to improve the condition of the system and to decrease the amount of parameters. Usually the nondimensionalization is done using an invariant transformation. In the case of a time varying radius of curvature R, load w or mean velocity u_m, the transformation is referenced to constant values R_{ref}, w_{ref} and u_{ref} (see e.g. [16]). This eventually yields a fixed reference frame, in which the pressurized contact zone may drastically change its extent: consequently, the solutions will have very low similarity and therefore, the reduction procedure might not be efficient anymore. In order to increase the similarity of the solutions, we adapt the nondimensionalization in such a way that the size of the corresponding dry contact remains the same within the dimensionless coordinates. The contact size is defined by the Hertzian half width or radius $a(R,w)$. With $a_{\text{ref}} = a(R_{\text{ref}}, w_{\text{ref}})$, the nondimensionalization is done by the transformation

$$\begin{aligned} &X = \frac{x}{a}, \quad Y = \frac{y}{a}, \quad P = \frac{p}{p_H}, \\ &H = \frac{hR}{a^2}, \quad H_0 = \frac{h_0 R}{a^2}, \quad \Delta = \frac{\delta R}{a^2}, \\ &\overline{\eta} = \frac{\eta}{\eta_0}, \quad \overline{\rho} = \frac{\rho}{\rho_0}, \quad \Lambda = \frac{R a_{\text{ref}}\lambda}{a^2 u_{\text{ref}}\rho_0}, \\ &U = \frac{a_{\text{ref}}u_m}{a u_{\text{ref}}}, \quad T = \frac{u_{\text{ref}}t}{a_{\text{ref}}} \end{aligned} \tag{6}$$

with Hertzian pressure $p_H(R,w)$ [17]. Since a_{ref} is calculated using reference values, it is constant with time. The reference values η_0 and ρ_0 are usually the viscosity and density for a pressure of zero. Introducing the transformation (6) into (1), the Reynolds equation

in dimensionless form is

$$\frac{\partial}{\partial X}\left(\varepsilon\frac{\partial P}{\partial X}\right)+\frac{\partial}{\partial Y}\left(\varepsilon\frac{\partial P}{\partial Y}\right)+\Lambda=U\frac{\partial\overline{\rho}H}{\partial X}+\frac{\partial\overline{\rho}H}{\partial T},$$
$$\Lambda\geq 0,\quad P\geq 0,\quad \Lambda\cdot P=0 \tag{7}$$

with

$$\varepsilon=\frac{\overline{\rho}H^3}{\overline{\eta}\overline{\lambda}}\quad\text{and}\quad\overline{\lambda}=\frac{12u_{\mathrm{ref}}\eta_0R^2}{p_ha^2a_{\mathrm{ref}}}.$$

Inserting (6) into (2) (5) yields for the line contact:

$$H(X,T)=H_0(T)+\frac{X^2}{2}+\Delta(X,T), \tag{8}$$

$$\int_{-\infty}^{+\infty}P(X,T)\,dX=\frac{\pi}{2}\quad\text{and} \tag{9}$$

$$\Delta(X,T)=\quad\frac{1}{2\pi}\int_{-\infty}^{+\infty}P(X',T)\ln((X\quad X')^2)\,dX'. \tag{10}$$

Using transformation (6), both the dimensionless film thickness equation (8) and the load balance (9) are parameter independent. So, the dimensionless solution is always given within a framework, which refers to its corresponding dry contact.

2.2. Discretization

Now, the time variant dimensionless problem is discretized in space and time. The EHD parameters at time step j are put together in the parameter vector

$$\boldsymbol{\mu}_j=[E',R|_j,u_m|_j,w|_j,\alpha,\eta_0] \tag{11}$$

Despite its time variance, the topology of the grid remains the same. Thus the inner nodes of the grid are stored in a lexicographical order, concatenating all rows in the x direction. However, within this work there is the need of accessing only a particular set of nodes. Therefore, we introduce the following notation to denote a submatrix of a matrix $\boldsymbol{A}\in\mathbb{R}^{n\times m}$:

$$\overset{\mathcal{M}}{\mathcal{N}}\boldsymbol{A}=\begin{bmatrix}A_{n_1m_1}&\cdots&A_{n_1m_{\hat{m}}}\\ \vdots&\ddots&\vdots\\ A_{n_{\hat{n}}m_1}&\cdots&A_{n_{\hat{n}}m_{\hat{m}}}\end{bmatrix}\in\mathbb{R}^{\hat{n}\times\hat{m}}, \tag{12}$$

whereupon the indices of the submatrix are merged in the sets

$\mathcal{N}=\{n_1,\ldots,n_{\hat{n}}\}\subseteq\{1,\ldots,n\}$ and
$\mathcal{M}=\{m_1,\ldots,m_{\hat{m}}\}\subseteq\{1,\ldots,m\}$

with number of entries $|\mathcal{N}|=\hat{n}$ and $|\mathcal{M}|=\hat{m}$. Thereby, the operator $|\cdot|$ returns the number of elements of a set. The notation is also valid for one dimension only.

The EHD problem is solved by using a full system approach [18]. Therefore the dimensionless values for pressure P, deformation Δ and Lagrangian multiplier Λ of all inner nodes at time step j are gathered in column matrices $\boldsymbol{p}_j$, $\boldsymbol{\delta}_j$ and λ_j, respectively. Therewith, the state vector for the full system is

$$\boldsymbol{z}_j=[\boldsymbol{p}_j^T,\boldsymbol{\delta}_j^T,H_{0j}]^T. \tag{13}$$

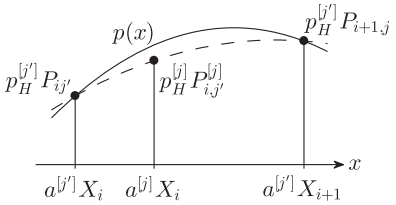

Fig. 1. Interpolation of the dimensionless pressure P from framework [j'] to [j] in the physical space.

The Reynolds equation (1) is discretized by finite differences using a standard discretization scheme [3]. It includes second order central differences for the second order derivatives and, due to numerical stability reasons, second order backward differences for the first order derivatives of the convective parts. So, at the jth time step the discretized nonlinear Reynolds equation $\boldsymbol{f}_{\boldsymbol{p}j}$, following from the first part of (7), can be written as

$$\boldsymbol{f}_{\boldsymbol{p}j}(\boldsymbol{z}_j,\boldsymbol{z}_{j-1}^{[j]},\boldsymbol{z}_{j-2}^{[j]},\boldsymbol{\mu}_j)+\lambda_j=\boldsymbol{0}. \tag{14}$$

Since a second order backward difference is used for the time derivative, the function is dependent on the solutions of the last two time steps. Furthermore, as the dimensionless framework is different in every time step, the solution $\boldsymbol{z}_{j'}$ of a prior time step j' has to be projected to the current framework at time step j. Thereby, the superscript [$\cdot$] indicates the framework to which it is projected. If framework and time step coincide, the superscript is omitted. The transformation from framework [j'] to [j] is done by a transformation $\boldsymbol{g}$:

$$\boldsymbol{z}_{j'}^{[j]}=\boldsymbol{g}(\boldsymbol{z}_{j'},\boldsymbol{\mu}_{j'},\boldsymbol{\mu}_j). \tag{15}$$

As Fig. 1 shows, the transformation $\boldsymbol{g}$ contains both an extension of size and an interpolation in spatial direction. Here a cubic spline interpolation turns out to be an adequate method. For the sake of simplicity, the dependency on former time steps and the parameter dependency will not be stated explicitly in the following.

Both, the elasticity equation (10) and the load balance (9) are linear. In discrete form, they can be written as

$$\boldsymbol{f}_{\boldsymbol{\delta}_j}(\boldsymbol{z}_j)=\boldsymbol{\delta}_j\quad\boldsymbol{K}\boldsymbol{p}_j=\boldsymbol{0}\quad\text{and} \tag{16}$$

$$f_{h_{0_j}}(\boldsymbol{z}_j)=c_{h_0}\quad\boldsymbol{K}_{h_0}\boldsymbol{p}_j=0. \tag{17}$$

Hereby, the flexibility matrix $\boldsymbol{K}$ can be found e.g. in [3] for the point contact and in [19] for the line contact.

To cope with the complementarity problem in (7), an active set procedure will be used [20]. Therefore, the discrete complementarity problem is reformulated as

$$\lambda_{ij}\quad\max(0,\lambda_{ij}\quad cp_{ij})=0, \tag{18}$$

where c is a positive constant, coping with possible different units or sizes of the two protagonists. Therewith, the case of occurrence of film rupture ($\lambda_{ij}>0,p_{ij}=0$) can be expressed by

$$\lambda_{ij}\quad cp_{ij}>0. \tag{19}$$

So, the indices of all $2n+1$ equations are partitioned into an active set $\mathcal{A}$, where the film ruptures, and a passive set $\mathcal{P}$, where pressure is generated. The sets are defined by

$$\mathcal{A}:=\{i\in\{1,\ldots,n\}:\lambda_{ij}\quad cp_{ij}>0\}, \tag{20}$$

$$\mathcal{P}:=\{1,\ldots,2n+1\}\backslash\mathcal{A}. \tag{21}$$

Since the complementarity problem is only employed in the Reynolds equation, only the first n equations can be candidates.

Finally, the solution of the EHD contact problem is calculated iteratively using a damped Newton Raphson method. With the notation defined in Section 2.2, the iteration scheme reads

$${}_{\mathcal{P}}\boldsymbol{z}_j^{(k)}={}_{\mathcal{P}}\boldsymbol{z}_j^{(k-1)}+\omega_{\mathcal{P}}\Delta\boldsymbol{z}_j^{(k)}, \tag{22}$$

with $0<\omega\leq 1$. The change in the kth iteration arises out of solving the linearized equation system

$$\begin{bmatrix}{}_{\mathcal{P}}^{\mathcal{P}}\boldsymbol{J}_{\boldsymbol{f}j}^{(k-1)}\boldsymbol{0}\\ {}_{\mathcal{A}}^{\mathcal{P}}\boldsymbol{J}_{\boldsymbol{f}j}^{(k-1)}\boldsymbol{1}\end{bmatrix}\begin{bmatrix}{}_{\mathcal{P}}\Delta\boldsymbol{z}_j^{(k)}\\ {}_{\mathcal{A}}\lambda_j^{(k)}\end{bmatrix}=\quad\begin{bmatrix}{}_{\mathcal{P}}\boldsymbol{f}_j^{(k-1)}\\ {}_{\mathcal{A}}\boldsymbol{f}_j^{(k-1)}\end{bmatrix} \tag{23}$$

with function $\boldsymbol{f}=[\boldsymbol{f}_{\boldsymbol{p}}^T,\boldsymbol{f}_{\boldsymbol{\delta}}^T,f_{h_0}]^T$ and its Jacobian $\boldsymbol{J}_{\boldsymbol{f}}$. Following from the complementarity problem the remaining unknowns ${}_{\mathcal{A}}\boldsymbol{z}_j^{(k)}$ and

${}_{\mathcal{P}}\lambda_j^{(k)}$ are zero. The sets $\mathcal{A}$ and $\mathcal{P}$ have to be updated in every iteration. Nevertheless, the size of the equation system (23) remains constant. The algorithm terminates when $\|{}_{\mathcal{P}}\boldsymbol{f}_j\|_2$ is smaller than a particular threshold, which is chosen to fulfill a desired accuracy.

3. Reduction of the EHD contact

The idea of projection based model order reduction [21] methods is to approximate the input output behavior of a parametric and/or dynamical system by a much smaller subspace. The procedure is divided into an offline and online phase. In the former, which is performed only once, the reduced system is created. The latter is repeated very often and consists of solving the reduced model. In particular, the method gets efficient when no large scaled operations are necessary within the online phase. In order to reach this efficiency, three steps of reduction have to be accomplished. The first is the reduction of the large scale system of size n. The second step contains a gappy evaluation of the $\{2n+1\}\times 1$ system function and the $n\times\{2n+1\}$ nonlinear sparse part of its Jacobian. The last step of reduction consists of a local evaluation of the complementarity problem.

3.1. Reduction of the system

The reduction of the system is done by projecting its linearized version (23) to a smaller subspace. Therefore, the unknown part of the state vector is approximated by the trial base $\boldsymbol{V}\in\mathbb{R}^{\{2n+1\}\times\tilde{n}}$ of shape functions with $\tilde{n}\ll n$:

$${}_{\mathcal{P}}\boldsymbol{z}\approx{}_{\mathcal{P}}\boldsymbol{V}\tilde{\boldsymbol{z}} \tag{24}$$

Introducing (24) into the first part of (23) and left multiplication of the transpose of the test basis $\boldsymbol{W}\in\mathbb{R}^{\{2n+1\}\times\tilde{n}}$ of weighting functions leads to the reduced equation

$${}_{\mathcal{P}}\boldsymbol{W}^T{}_{\mathcal{P}}{}^{\mathcal{P}}\boldsymbol{J}_{\boldsymbol{f}j}^{(k-1)}{}_{\mathcal{P}}\boldsymbol{V}\Delta\tilde{\boldsymbol{z}}_j^{(k)}=\quad{}_{\mathcal{P}}\boldsymbol{W}^T{}_{\mathcal{P}}\boldsymbol{f}_j^{(k-1)}. \tag{25}$$

For the trial basis, independent basis functions for pressure and deformation are used:

$$\boldsymbol{V}=\operatorname{diag}(\boldsymbol{V}_{\boldsymbol{p}},\boldsymbol{V}_{\boldsymbol{\delta}},1)\in\mathbb{R}^{\{2n+1\}\times\{\tilde{n}_p+\tilde{n}_\delta+1\}}. \tag{26}$$

The basis functions follow from applying snapshot POD [22] to a sufficiently large set of solutions, obtained by solving the full problem for different trajectories or parameter combinations. Hereby, proper orthogonal decomposition (POD) provides an orthonormal basis spanning the vector space of incoming vectors best in the sense of the Euclidean norm.

For the test basis, a weighted form of the matrix multiplication of Jacobian and trial basis is used:

$$\boldsymbol{W}=\boldsymbol{D}^2\boldsymbol{J}_{\boldsymbol{f}}\boldsymbol{V}. \tag{27}$$

Since the entries of the sparse sub Jacobian $\boldsymbol{J}_{\boldsymbol{f}_{\boldsymbol{p}}}$, corresponding to the Reynolds equation, are much smaller in the rows representing the center of the contact than those outside, the diagonal matrix $\boldsymbol{D}$ is introduced. Its pre multiplication counteracts the bad conditioning of $\boldsymbol{J}_{\boldsymbol{f}_{\boldsymbol{p}}}$. Various tests have shown that an adequate choice of $\boldsymbol{D}$ is to use the identity matrix and replace the entries corresponding to pressure by the first POD basis function for pressure.

Solving Eq. (25) for $\Delta\tilde{\boldsymbol{z}}_j^{(k)}$, the iteration scheme (22) can be written in reduced form as

$$\tilde{\boldsymbol{z}}_j^{(k)}=\tilde{\boldsymbol{z}}_j^{(k-1)}\quad\omega\tilde{\boldsymbol{J}}^+\tilde{\boldsymbol{f}} \tag{28}$$

with pseudoinverse $\tilde{\boldsymbol{J}}^+=(\tilde{\boldsymbol{J}}^T\tilde{\boldsymbol{J}})^{-1}\tilde{\boldsymbol{J}}^T$ and matrices

$$\tilde{\boldsymbol{f}}={}_{\mathcal{P}}^{\tilde{\mathcal{P}}}\boldsymbol{D}_{\mathcal{P}}\boldsymbol{f}_j^{(k-1)}\quad\text{and} \tag{29}$$

$$\tilde{\boldsymbol{J}}={}_{\mathcal{P}}^{\tilde{\mathcal{P}}}\boldsymbol{D}_{\mathcal{P}}{}^{\mathcal{P}}\boldsymbol{J}_{\boldsymbol{f}j}^{(k-1)}{}_{\mathcal{P}}\boldsymbol{V}. \tag{30}$$

Here, only a small matrix of size $\tilde{n}\times\tilde{n}$ has to be inverted. Nevertheless, the evaluation of $\tilde{\boldsymbol{f}}$ and $\tilde{\boldsymbol{J}}$, as well as the matrix multiplications $\tilde{\boldsymbol{J}}^T\tilde{\boldsymbol{f}}$ and $\tilde{\boldsymbol{J}}^T\tilde{\boldsymbol{J}}$ is still of order n. The following subsection deals with how to overcome this problem.

3.2. Reduction of system evaluation

The reduction of evaluation of the system matrices is achieved by a condensation and negligence of equations of the highly overdetermined least square problem of (28). Introducing the set

$$\tilde{\mathcal{P}}:=\{1,\ldots,n\}\backslash\mathcal{A} \tag{31}$$

the expressions (29) and (30) can be given in detail as

$$\tilde{\boldsymbol{f}}=\begin{bmatrix}{}_{\mathcal{P}}^{\tilde{\mathcal{P}}}\boldsymbol{D}_{\tilde{\mathcal{P}}}\boldsymbol{f}_{\boldsymbol{p}j}^{(k-1)}\\ \boldsymbol{f}_{\boldsymbol{\delta}j}^{(k-1)}\\ f_{h_0j}^{(k-1)}\end{bmatrix}\in\begin{bmatrix}\mathbb{R}^{|\tilde{\mathcal{P}}|}\\ \mathbb{R}^n\\ \mathbb{R}\end{bmatrix}\quad\text{and} \tag{32}$$

$$\tilde{\boldsymbol{J}}=\begin{bmatrix}{}_{\mathcal{P}}^{\tilde{\mathcal{P}}}\boldsymbol{D}_{\tilde{\mathcal{P}}}{}^{\mathcal{P}}\boldsymbol{J}_{\boldsymbol{f}_{\boldsymbol{p}}j}^{(k-1)}{}_{\mathcal{P}}\boldsymbol{V}\\ {}^{\mathcal{P}}\boldsymbol{J}_{f_\delta\mathcal{P}}\boldsymbol{V}\\ {}^{\mathcal{P}}J_{f_{h_0}\mathcal{P}}\boldsymbol{V}\end{bmatrix}\in\begin{bmatrix}\mathbb{R}^{|\tilde{\mathcal{P}}|\times\tilde{n}}\\ \mathbb{R}^{n\times\tilde{n}}\\ \mathbb{R}^{1\times\tilde{n}}\end{bmatrix}. \tag{33}$$

The condensation is done for the linear elasticity part by pre multiplication of $\boldsymbol{V}_{\boldsymbol{\delta}}^T$:

$$\tilde{\boldsymbol{f}}^{\mathrm{I}}=\begin{bmatrix}{}_{\mathcal{P}}^{\tilde{\mathcal{P}}}\boldsymbol{D}_{\tilde{\mathcal{P}}}\boldsymbol{f}_{\boldsymbol{p}j}^{(k-1)}\\ \boldsymbol{V}_{\boldsymbol{\delta}}^T\boldsymbol{f}_{\boldsymbol{\delta}j}^{(k-1)}\\ f_{h_0j}^{(k-1)}\end{bmatrix}\in\begin{bmatrix}\mathbb{R}^{|\tilde{\mathcal{P}}|}\\ \mathbb{R}^{\tilde{n}_\delta}\\ \mathbb{R}\end{bmatrix}\quad\text{and} \tag{34}$$

$$\tilde{\boldsymbol{J}}^{\mathrm{I}}=\begin{bmatrix}{}_{\mathcal{P}}^{\tilde{\mathcal{P}}}\boldsymbol{D}_{\tilde{\mathcal{P}}}{}^{\mathcal{P}}\boldsymbol{J}_{\boldsymbol{f}_{\boldsymbol{p}}j}^{(k-1)}{}_{\mathcal{P}}\boldsymbol{V}\\ \boldsymbol{V}_{\boldsymbol{\delta}}^T{}^{\mathcal{P}}\boldsymbol{J}_{f_\delta\mathcal{P}}\boldsymbol{V}\\ {}^{\mathcal{P}}J_{f_{h_0}\mathcal{P}}\boldsymbol{V}\end{bmatrix}\in\begin{bmatrix}\mathbb{R}^{|\tilde{\mathcal{P}}|\times\tilde{n}}\\ \mathbb{R}^{\tilde{n}_\delta\times\tilde{n}}\\ \mathbb{R}^{1\times\tilde{n}}\end{bmatrix}. \tag{35}$$

Since elasticity equation and load balance are linear, its Jacobians are actually constant. However, the reduced Jacobians in Eq. (35) are changing, when entries are added to or subtracted from set $\mathcal{P}$. If a node $i\notin\mathcal{P}$ is added to $\mathcal{P}$, the reduced Jacobian of the elasticity equation can be updated by

$$\boldsymbol{V}_{\boldsymbol{\delta}}^{T\mathcal{P}\cup\{i\}}\boldsymbol{J}_{f_\delta\mathcal{P}\cup\{i\}}\boldsymbol{V}=\boldsymbol{V}_{\boldsymbol{\delta}}^{T\mathcal{P}}\boldsymbol{J}_{f_\delta\mathcal{P}}\boldsymbol{V}+{}^{\{i\}}(\boldsymbol{V}_{\boldsymbol{\delta}}^T\boldsymbol{J}_{f_\delta})_{\{i\}}\boldsymbol{V}. \tag{36}$$

The subtraction of a node is straightforward. Equivalently, this can be done for the reduced Jacobian of the load balance equation.

Finally, the evaluation of the nonlinear part is reduced by a system approximation based on [23]. Therefore only the $\hat{n}\ll n$ most important rows of the Reynolds equation, defined by index set $\mathcal{I}$ with $|\mathcal{I}|=\hat{n}$, are taken for the least squares problem. For that, all training calculations, done to get the trial basis, are repeated with the reduced system on level I. Snapshots of the first part of

Table 1
WFL parameters for lubricant no. 1 and no. 2 from [25] and for no. 3 from [26].

Parameter	No. 1	No. 2	No. 3
A_1 (°C)	19.17	22.47	69.81
A_2 (GPa $^{-1}$)	4.07	4.22	1.68
B_1	0.230	0.222	0.213
B_2 (MPa $^{-1}$)	0.0249	0.0349	0.0118
C_1	16.04	15.87	11.84
C_2 (°C)	18.18	10.22	60.59
$T_g(0)$ (°C)	−73.86	−113.79	−87.46
μ_g (Pa s)	10^{12}	10^{12}	10^7

L \ M	LLR 5	8	10	12	15	17	20	25	30	35	40	50	HLR 50	58	67	77	88	102	118	136	157	181	208	240	277	319	368	425	490	565	652	752	867	1000
1	×	×	×	×	×	×	×	×	×	×	×	×		×		×		×		×		×		×		×		×		×		×	
3	×	×	×	×	×	×	×	×	×	×	×	×	×		×		×		×		×		×		×		×		×		×		×
5	×	×	×	×	×	×	×	×	×	×	×	×		×		×		×		×		×		×		×		×		×		×	
7	×	×	×	×	×	×	×	×	×	×	×	×	×		×		×		×		×		×		×		×		×		×		×
9	×	×	×	×	×	×	×	×	×	×	×	×		×		×		×		×		×		×		×		×		×		×	
11	×	×	×	×	×	×	×	×	×	×	×	×	×		×		×		×		×		×		×		×		×		×		×
13	×	×	×	×	×	×	×	×	×	×	×	×		×		×		×		×		×		×		×		×		×		×	
15	×	×	×	×	×	×	×	×	×	×	×	×	×		×		×		×		×		×		×		×		×		×		×
17	×	×	×	×	×	×	×	×	×	×	×	×		×		×		×		×		×		×		×		×		×		×	
20	×	×	×	×	×	×	×	×	×	×	×	×	×		×		×		×		×		×		×		×		×		×		×

Fig. 2. Selected snapshots for POD bases for lower loaded LLR (left) and higher loaded region HLR (right).

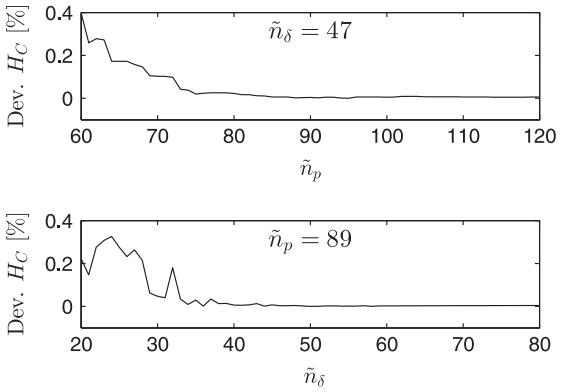

Fig. 3. Deviation of central film thickness between full and reduced model subject to the number of basis function for pressure (upper) and elastic deformation (lower) for test case M 12, L 12 and p_H 0.7 GPa using lubricant no. 1.

Table 2
Degrees of freedom for the stationary case.

Region	n	$2n+1$	m	$\tilde{n}$	$\tilde{n}_p$	$\tilde{n}_\delta$	$\hat{n}$	$\check{n}$
LLR	1201	2403	120	137	89	47	160	290
HLR	3001	6003	110	113	80	32	160	339

(34) and the product of the first part of (35) and the solution at iteration k are collected for every iteration, for every time step of every training. Applying POD on the snapshot matrices, the POD bases $\boldsymbol{\Phi}_{\tilde{\boldsymbol{f}}}$ and $\boldsymbol{\Phi}_{\boldsymbol{j}}$ are obtained. The algorithm on how to determine $\mathcal{I}$ out of these POD bases can be found in the appendix. The $\check{n}$ indices of state variables, which are necessary to evaluate the $\hat{n}$ rows given by $\mathcal{I}$, are combined within the set $\mathcal{J}$ with $|\mathcal{J}| = \check{n}$. Usually, since the discretization scheme for the Reynolds equation is local, it is also $\check{n} \ll n$. To cope with the complementarity problem, the sets $\tilde{\mathcal{I}} := \mathcal{I} \backslash \mathcal{A}$ and $\tilde{\mathcal{J}} := \mathcal{J} \backslash \mathcal{A}$ are introduced. Therewith the matrices for the fully reduced system read

$$\tilde{\boldsymbol{f}}^{\mathrm{II}} = \begin{bmatrix} {}^{\tilde{\mathcal{I}}}\boldsymbol{D}_{\tilde{\mathcal{I}}} \boldsymbol{f}_{\boldsymbol{p}j}^{(k-1)} \\ \boldsymbol{V}_{\boldsymbol{\delta}}^T \boldsymbol{f}_{\boldsymbol{\delta}j}^{(k-1)} \\ f_{h_0 j}^{(k-1)} \end{bmatrix} \in \begin{bmatrix} \mathbb{R}^{|\tilde{\mathcal{I}}|} \\ \mathbb{R}^{\tilde{n}_\delta} \\ \mathbb{R} \end{bmatrix} \quad \text{and} \tag{37}$$

$$\tilde{\boldsymbol{J}}^{\mathrm{II}} = \begin{bmatrix} {}^{\tilde{\mathcal{I}}}\boldsymbol{D}_{\tilde{\mathcal{I}}} {}^{\tilde{\mathcal{J}}}\boldsymbol{J}_{\boldsymbol{f}_{\boldsymbol{p}}\boldsymbol{j}}^{(k-1)} {}_{\tilde{\mathcal{J}}}\boldsymbol{V} \\ \boldsymbol{V}_{\boldsymbol{\delta}}^{T\,\mathcal{P}}\boldsymbol{J}_{f_\delta \mathcal{P}} \boldsymbol{V} \\ {}^{\mathcal{P}}J_{f_{h_0}\mathcal{P}} \boldsymbol{V} \end{bmatrix} \in \begin{bmatrix} \mathbb{R}^{|\tilde{\mathcal{I}}| \times \tilde{n}} \\ \mathbb{R}^{\tilde{n}_\delta \times \tilde{n}} \\ \mathbb{R}^{1 \times \tilde{n}} \end{bmatrix}. \tag{38}$$

With these approximations, only matrix evaluations, additions and multiplication with size $\hat{n}$, $\check{n}$ and $\tilde{n}$ are necessary.

Table 3
Comparison of performance between full and reduced model.

Parameter			Num. of iter.		Calc. time (s)	
M	L	p_H (GPa)	Full	Red.	Full	Red.
No. 1						
12	12	0.70	5	6	1.25	0.024
17	15	1.04	4	4	1.00	0.016
45	5	0.57	5	5	1.24	0.019
100	10	1.69	5	5	14.6	0.020
600	8	3.31	5	5	14.6	0.017
No. 2						
13	8	0.92	6	8	1.49	0.031
40	9	1.82	5	5	1.24	0.019
45	5	1.07	5	6	1.27	0.022
120	10	3.50	5	7	14.5	0.024
500	6	4.28	4	15	11.6	0.048
No. 3						
12	8	0.61	5	5	1.25	0.019
18	15	1.41	6	9	1.50	0.036
40	12	1.68	5	7	1.25	0.028
200	12	3.75	5	5	14.6	0.017
600	6	3.25	4	13	11.6	0.041

3.3. Reduction of the complementarity problem

For the last part the assumption is made that the film rupture occurs at the outlet and there is no pressure generation down stream. So there exists one connected boundary between ruptured and pressurized area, which can be expressed as $x = f(y)$. Instead of ${}_{\mathcal{A}}\boldsymbol{\lambda}_j$, only ${}_{\mathcal{B}}\boldsymbol{\lambda}_j$ are calculated. Thereby, the set $\mathcal{B}$, which indicates the film rupture, is defined by

$$\mathcal{B} := \{i \in \mathcal{A} : i \quad 1 \in \mathcal{P}\}. \tag{39}$$

So, the number of entries of $\mathcal{B}$ is equal to the number of nodes in the y direction. Since a light misestimation of $\mathcal{B}$ is not crucial for the solution, further reduction might be possible by a gappy evaluation and interpolation in the y direction. The adaption of $\mathcal{B}$ and therewith of $\mathcal{A}$ and $\mathcal{P}$ takes place in every iteration. If a negative pressure is detected before the exit boundary, the particular index of $\mathcal{B}$ is decremented in the x direction. Otherwise the particular index is incremented, if the inequality condition (19) is fulfilled. In order to avoid oscillatory behavior of the border, the adaption might be aborted after a specified amount of iterations. This number should be higher than the number of nodes the exit boundary moves within one time step.

4. Results

The EHD reduction method, described in Section 3, is applied to a stationary and a transient EHD line contact problem. Stationary means that the last term on the right side of Eq. (7) is omitted.

Table 4
Comparison of full and reduced solutions of central film thickness for different parameters.

Parameter			H_C (Habchi et al. [12])			H_C (Current model)			Model Dev. (‰)
M	L	p_H (GPa)	Full	Red.	Dev. (‰)	Full	Red.	Dev. (‰)	
No. 1									
12	12	0.70	0.18052049	0.18052302	0.014	0.17966418	0.17965820	0.033	4.766
17	15	1.04	0.13772694	0.13771578	0.081	0.13701194	0.13701770	0.042	5.218
45	5	0.57	0.02515687	0.02515679	0.003	0.02515764	0.02515528	0.094	0.031
100	10	1.69	0.01438153	0.01438083	0.049	0.01437200	0.01437152	0.033	0.663
600	8	3.31	0.00159831	0.00159830	0.006	0.00157085	0.00157081	0.023	17.48
No. 2									
13	8	0.92	0.13077684	0.13074332	0.256	0.13029989	0.13047942	1.378	3.660
40	9	1.82	0.03846414	0.03847607	0.310	0.03837291	0.03835223	0.539	2.378
45	5	1.07	0.02465579	0.02458083	3.040	0.02455470	0.02457322	0.754	4.117
120	10	3.50	0.01165195	0.01166741	1.327	0.01163337	0.01162762	0.494	1.597
500	6	4.28	0.00166994	0.00167389	2.365	0.00164452	0.00164732	1.702	15.46
No. 3									
12	8	0.61	0.14334110	0.14334916	0.056	0.14277281	0.14273619	0.257	3.980
18	15	1.41	0.12726978	0.12728937	0.154	0.12720192	0.12720041	0.012	0.534
40	12	1.68	0.04516983	0.04519063	0.460	0.04513897	0.04512421	0.327	0.684
200	12	3.75	0.00719969	0.00720202	0.324	0.00718491	0.00718138	0.491	2.058
600	6	3.25	0.00133440	0.00133627	1.401	0.00130920	0.00131040	0.919	19.25

Table 5
Properties from [9].

E' (GPa)	R (m)	η_0 (Pa s)	α (GPa $^{-1}$)
287.8	0.0225	0.004	22

Table 6
Degrees of freedom for the transient case.

n	m	n	n_p	n_δ	$\hat{n}$	n
1201	11,915	175	87	87	148	401

The first test gives a comparison to the results shown in [12]. Therefore, the pressure viscosity dependency is modeled by a modified WLF model given by [24]:

$$\begin{aligned}&\eta(p)=\mu_g\cdot 10^{(-C_1\cdot(T_0-T_g(p))D(p))/(C_2+(T_0-T_g(p))D(p))}\ \text{with}\\&T_g(p)=T_g(0)+A_1\ln(1+A_2p)\ \text{and}\\&D(p)=1\quad B_1\ln(1+B_2p).\end{aligned}\tag{40}$$

The Dowson and Higginson model [1] is used to get the pressure density relation. In Table 1 the WLF parameters for three different lubricants are listed. The dimensionless computational area $\{\ -4\le X\le 2\}$ is discretized equidistantly. The Moes parameter space is divided into a lower loaded region (LLR) with a step size of $h_X=0.005$ and a higher loaded region (HLR) with a step size of $h_X=0.002$. Fig. 2 shows the distribution of the particular m snap shots in those two regions. As in [12] the snapshots are calculated for lubricant no. 1. Nevertheless, since the spatial shape of pressure is more complex than one of the deformations, the calculation of more snapshots than proposed in [12] was necessary. Even though m might not be small, the number of basis functions for the reduced system may be much smaller after the application of snapshot POD. Fig. 3 shows the increase of accuracy with an increasing number of basis functions. However, there is no further improvement of accuracy after a specified amount of basis func tions. So the number of basis function is chosen in such a way that the necessary accuracy is just fulfilled. Table 2 lists the sizes of the full and the reduced model for the two regions given in Fig. 2.

In order to test the accuracy and the efficiency of the reduced EHD contact model, 15 test cases from [12] using the lubricants given in Table 1 are considered. The number of iterations and the total calculation time for the full and the reduced model for the different test cases are given in Table 3. The starting solution of each test case is the solution of the trainings illustrated in Fig. 2 with the lowest Euclidean distance in the M L space. All calculations were done with Matlab using an i5 2500 CPU. The given time measurements are mean values. Since a self implemented Matlab code is used, the efficiency might not be competitive to professional, highly specialized solvers. However, the results clearly show a strong decrease of calculational time between the reduced and the full system.

Finally, Table 4 lists dimensionless central film thickness results of the reduced and the full model given in [12] and the one of the current models, together with the deviations between full and reduced model as well as the deviation between the full models itself. For all tests, the deviation of the central film thickness between the full and the reduced system is around or below one tenth of a percent and stays within the deviations due to model ing. However, the accuracy of the reduced system strongly depends on the choice of snapshots. Indeed, the reduced solutions are very good for the parameter combinations using lubricant no. 1, which was used for training. So, in order to get a reliable and accurate reduced model in a specified parameter range, there has to be spent a lot of effort in the selection of the snapshots.

The next example refers to the transient EHD line contact calculations given in [9] with Moes parameters $M=120$ and $L=10$ and the same material, geometry and fluid properties given in Table 5. The lubricant is modeled as incompressible with a Barus viscosity pressure relationship [27]. The load w is varied sinu soidally with

$$w=w_{\text{ref}}\left[1+\frac{1}{10}\sin\left(\frac{2\pi T}{T_{\text{excitation}}}\right)\right]\tag{41}$$

for different period times $T_{\text{excitation}}$. As trainings for the reduced model, the running in from stationary position up to “stationary” transient behavior for

$$T_{\text{excitation}}\in\left\{\frac{1}{2}\frac{a_{\text{ref}}}{u_{\text{ref}}},\frac{a_{\text{ref}}}{u_{\text{ref}}},2\frac{a_{\text{ref}}}{u_{\text{ref}}}\right\}\tag{42}$$

is used. The dimensions for the transient reduced model are summarized in Table 6. The time integration is done with an

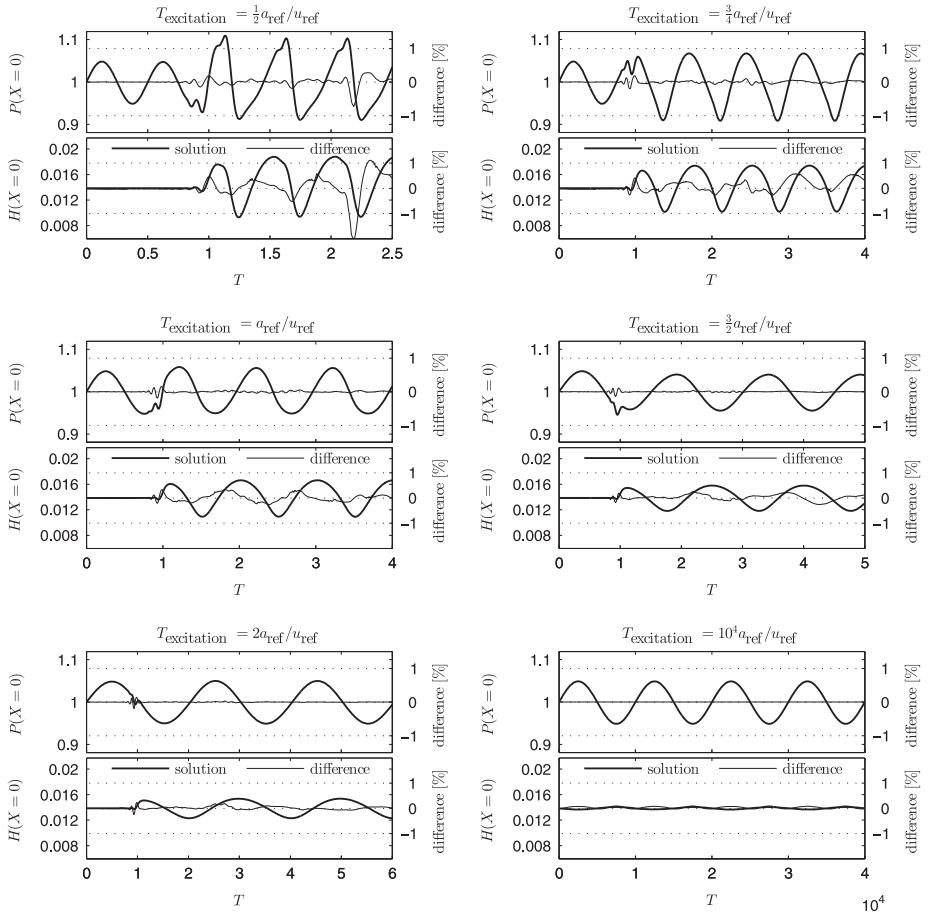

Fig. 4. Solution of central pressure and film thickness given in a constant reference and the relative difference of full to reduced solution.

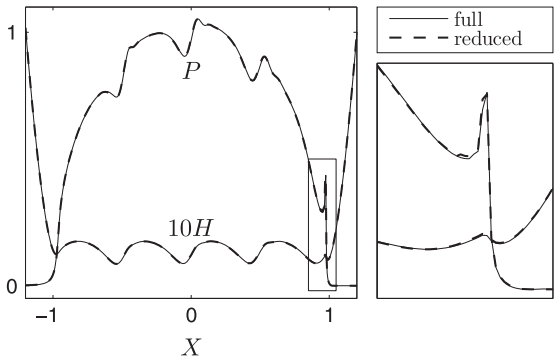

Fig. 5. Dimensionless pressure and film thickness distribution within contact and at the outlet region for $T_{\text{excitation}}$ $1/2\ a_{\text{ref}}/u_{\text{ref}}$ at T 2.185.

Table 7
Dimensions of time integration.

Trajectory, $T_{\text{excitation}}$	Num. of time steps		Calc. time (s)	
	Full	Red.	Full	Red.
$1/2\ a_{\text{ref}}/u_{\text{ref}}$	5010	4192	3949	119
$3/4\ a_{\text{ref}}/u_{\text{ref}}$	5419	4465	4156	131
$a_{\text{ref}}/u_{\text{ref}}$	3914	3506	3053	91
$3/2\ a_{\text{ref}}/u_{\text{ref}}$	3409	2647	2624	62
$2a_{\text{ref}}/u_{\text{ref}}$	2991	2478	2368	56
$10^4 a_{\text{ref}}/u_{\text{ref}}$	3653	3169	2710	94

adaptive time stepping scheme, using the local error prediction suggested in [28]. Fig. 4 shows the results of dimensionless central pressure and film thickness with time of the full solution and the difference between full and reduced solution in percent. The difference between full and reduced solution decreases with increasing $T_{\text{excitation}}$. Remarkably, this statement is valid indepen dent from the fact whether or not the trajectory has been one of the training sets. The maximum differences are generated due to a time shift and not due to the prediction of a wrong value. An indicator therefore is the fact that the maximum differences occur, when the time derivative of the solution maximizes. Fig. 5 gives the dimensionless pressure and film thickness distribution within the contact for $T_{\text{excitation}} = 1/2\ a_{\text{ref}}/u_{\text{ref}}$ at time T=2.185, where the error reaches a maximum. Additionally, a zoom in of the outlet region is given on the right.

The quasi stationary case $T_{\text{excitation}} = 10,000 a_{\text{ref}}/u_{\text{ref}}$ shows a very good agreement, even though the excitation frequency time is beyond the trained zone. Table 7 lists the number of time steps and the total calculation time of the corresponding trajectory for the full and the reduced system. The number of necessary time steps depends on the local error tolerance and is similar for the time integration of the full and the reduced system.

5. Discussion

As mentioned above, model order reduction relies on the simi larity of the solution space, since global basis functions superpose the solution. Thus the method is especially efficient for a highly loaded

contact, where the solutions of pressure are similar to the Hertzian pressure distribution. Furthermore, the modeling of the lubricant has a strong influence on the efficiency of the method, since it affects the distinctness of the pressure spike at the outlet. So, the approach works better for a compressible lubricant with a smooth peak than for an incompressible lubricant. The same applies for Roelands viscosity in comparison to Barus viscosity.

For the transient case, an additional source of dissimilarity of the solution space is pressure waves, which are transported through the contact area by the lubricant. They occur if the excitation has a period time of less or around the characteristic time a/u_m. In particular, high amplitudes in conjunction with a period time below the character istic time are critical for the method.

An interesting point is the consideration of rough surfaces. The treatment of rough surfaces should be possible, as long as the surface can be described by a few parameters, entering the description base of the reduced order model. However, the method described in this work is supposed to be less effective, due to the highly amplified scattering of pressure distribution. A better outcome could possibly be expected, if the influence of rough surfaces is treated for example by using flow factors [29]. However, this investigation is beyond the scope of the paper.

As already included in the derivation of Sections 2 and 3, the method can also be applied to the EHD point contact problem. Further studies will test the efficiency and accuracy of this problem.

6. Conclusion

A model order reduction method is shown for the EHD line or point contact problem, including Reynolds equation, elasticity equation and load balance. The method consists of the generation of the reduced system and the solution of the reduced system. The former is called offline and the latter online phase. The reduction of the whole problem, nonlinear Reynolds and linear elasticity equation, is done in such a way that no operations of large size are necessary within the online phase. Therefore, the projected EHD problem is solved iteratively using a damped Newton Raphson scheme. The projection matrices are obtained by using snapshot POD and a problem specific test space approach, yielding a highly overdetermined least squares problem. This large scale least squares problem is approximated by a less complex one, which decreases the expenses for updating the system matrices. Finally, the complementarity problem is reduced by evaluating it locally and adapting the border of the exit boundary iteratively.

Moreover, a new nondimensionalization scheme for time varying parameters is introduced, which relates the computational area to the current size of the contact.

The results of the full and the reduced model match each other, for both the stationary and the transient case. Furthermore, the comparison of the results for the stationary EHD line contact problem with the results of former articles shows good accordance.

Acknowledgments

Kind acknowledgments go to the Robert Bosch GmbH for finan cial support and to the Université franco allemande for enabling the cotutelle.

Appendix A. Algorithm to determine $\mathcal{I}$

A simplified algorithm from [23] is given in Fig. A1.

Input: $\mathbf{\Phi}_{\tilde{f}}$, $\mathbf{\Phi}_{\tilde{\jmath}}$, $\hat{n}$
Output: $\mathcal{I}$

$$
\begin{aligned}
i &= \underset{j\in\{1,\dots,n\}}{\operatorname{argmax}} \left[{}^{\{1\}}_{\{j\}}\mathbf{\Phi}^2_{\tilde{f}} + {}^{\{1\}}_{\{j\}}\mathbf{\Phi}^2_{\tilde{\jmath}} \right] \\
\mathcal{I} &= \{i\} \\
&\text{for } \bar{n} = 2 : \hat{n} \\
&\quad \boldsymbol{a}_{\tilde{f}} = \underset{\boldsymbol{a}\in\mathbb{R}^{\bar{n}-1}}{\operatorname{argmin}} \left\| {}^{\{1,\dots,\bar{n}-1\}}_{\mathcal{I}}\mathbf{\Phi}_{\tilde{f}}\boldsymbol{a} - {}^{\{\bar{n}\}}_{\mathcal{I}}\mathbf{\Phi}_{\tilde{f}} \right\|_2 \\
&\quad \boldsymbol{a}_{\tilde{\jmath}} = \underset{\boldsymbol{a}\in\mathbb{R}^{\bar{n}-1}}{\operatorname{argmin}} \left\| {}^{\{1,\dots,\bar{n}-1\}}_{\mathcal{I}}\mathbf{\Phi}_{\tilde{\jmath}}\boldsymbol{a} - {}^{\{\bar{n}\}}_{\mathcal{I}}\mathbf{\Phi}_{\tilde{\jmath}} \right\|_2 \\
&\quad \boldsymbol{\varphi}_{\tilde{f}} = {}^{\{\bar{n}\}}\mathbf{\Phi}_{\tilde{f}} - {}^{\{1,\dots,\bar{n}-1\}}\mathbf{\Phi}_{\tilde{f}}\boldsymbol{a}_{\tilde{f}} \\
&\quad \boldsymbol{\varphi}_{\tilde{\jmath}} = {}^{\{\bar{n}\}}\mathbf{\Phi}_{\tilde{\jmath}} - {}^{\{1,\dots,\bar{n}-1\}}\mathbf{\Phi}_{\tilde{\jmath}}\boldsymbol{a}_{\tilde{\jmath}} \\
&\quad i = \underset{j\in\{1,\dots,n\}\setminus\mathcal{I}}{\operatorname{argmax}} \left[\left(\varphi_{\tilde{f},j}\right)^2 + \left(\varphi_{\tilde{\jmath},j}\right)^2 \right] \\
&\quad \mathcal{I} = \mathcal{I} \cup \{i\} \\
&\text{end}
\end{aligned}
$$

Fig. A1. Algorithm to determine $\mathcal{I}$.

References

[1] Dowson D, Higginson G. Elastohydrodynamic lubrication: the fundamentals of roller and gear lubrication. Oxford: Pergamon Press; 1966.
[2] Hamrock BJ, Dowson D. Isothermal elastohydrodynamic lubrication of point contacts. Part III: fully flooded results. ASME J Lubr Technol 1977;99:264–76.
[3] Venner CH, Lubrecht AA. Multilevel methods in lubrication, tribology series, vol. 37. Amsterdam: Elsevier; 2000.
[4] Moes H, Bosma R. Design charts for optimum bearing configuration. I: the full journal bearing. ASME J Tribol 1971;93:302–6.
[5] Hamrock BJ, Dowson D. Isothermal elastohydrodynamic lubrication of point contacts, part I: theoretical formulation. ASME 1976;98:223–9.
[6] Moes H. Optimum similarity analysis with applications to elastohydrodynamic lubrication. WEAR 1992;159:57–66.
[7] Grubin A. Investigation of the contact of machine components, vol. 30. Moscow: Central Scientific Research Institute for Technology and Mechanical Engineering (DSIR Translation 337); 1949.
[8] Morales-Espejel GE. Central film thickness in time-varying normal approach of rolling elastohydrodynamically lubricated contacts. Proc IMechE, Part C: J Mech Eng Sci 2008;222:1271–80.
[9] Félix-Quiñonez A, Morales-Espejel GE. Film thickness fluctuations in time-varying normal loading of rolling elastohydrodynamically lubricated contacts. Proc Inst Mech Eng, Part C: J Mech Eng Sci 2010;224(12):2559–67.
[10] Wiegert B, Hetzler H, Seemann W. A simplified elastohydrodynamic contact model capturing the nonlinear vibration behaviour. Tribol Int 2013;59:79–89.
[11] Habchi W, Issa J. A reduced full-system finite element approach to the solution of EHL problems: line contacts. In: ASME conference proceedings; 2010. p. 95–7.
[12] Habchi W, Issa J. Fast and reduced full-system finite element solution of elastohydrodynamic lubrication problems: line contacts. Adv Eng Softw 2013;56:51–62.
[13] Reynolds O. On the theory of lubrication and its application to Mr. Beauchamp tower's experiments, including an experimental determination of the viscosity of olive oil. Philos Trans R Soc Lond 1886;177:157–234.
[14] Flamant A. Sur la répartition des pressions dans un solide rectangulaire chargé transversalement. C R Acad Sci 1892;114:1465–8.
[15] Boussinesq J. Application des potentiels à l'étude de l'équilibre et du mouvement des solides élastiques. Paris: Gauthier-Villars; 1885.
[16] Messé S, Lubrecht A. Transient elastohydrodynamic analysis of an overhead cam/tappet contact. Proc Inst Mech Eng, Part J: J Eng Tribol 2000;214:415–25.
[17] Hertz H. Über die Berührung fester elastischer Körper. J reine angew Math 1881;92:156–71.
[18] Habchi W, Eyheramendy D, Vergne P, Morales-Espejel G. A full-system approach of the elastohydrodynamic line/point contact problem. J Tribol 2008;130(2):021501–10.
[19] Anuradha P, Kumar P. EHL line contact central and minimum film thickness equations for lubricants with linear piezoviscous behavior. Tribol Int 2011;44 (10):1257–60.
[20] Hager C, Wohlmuth BI. Semismooth newton methods for variational problems with inequality constraints. GAMM-Mitt 2010;33(1):8–24.
[21] Antoulas A. Approximation of large-scale dynamical systems. In: Advances in design and control. Philadelphia, PA: Society for Industrial and Applied Mathematics; 2005.
[22] Volkwein S. Proper orthogonal decomposition and singular value decomposition. Graz: Karl-Franzens-Universität Graz & Technische Universität Graz; 1999.
[23] Carlberg K, Bou-Mosleh C, Farhat C. Efficient nonlinear model reduction via a least-squares Petrov–Galerkin projection and compressive tensor approximations. Int J Numer Methods Eng 2011;86(2):155–81.
[24] Yasutomi S, Bair S, Winer WO. An application of a free volume model to lubricant rheology. I: dependence of viscosity on temperature and pressure. ASME J Tribol 1984;106:291–312.

[25] Molimard J, Querry M, Vergne P. Lubricant rheology in real conditions: measurements and confrontation with a ball/disk contact. Rev Métall 2001;98:141–8.
[26] Nélias D, Legrand E, Vergne P, Mondier J. Traction behavior of some lubricants used for rolling bearings in spacecraft applications: experiments and thermal model based on primary laboratory data. J Tribol 2001;124:72–81.
[27] Barus C. Isothermal, isopiestics, and isometrics relative to viscosity. Am J Sci 1893;45:87–96.
[28] Goodyer CE. Adaptive numerical methods for elastohydrodynamic lubrication [Ph.D. thesis]. University of Leeds; 2001.
[29] Patir N, Cheng HS. Application of average flow model to lubrication between rough sliding surfaces. J Lubr Technol 1979;101(2):220–9.